Available online at www.sciencedirect.com

SciVerse ScienceDirect

Journal of the European Ceramic Society 32 (2012) 2731–2738

www.elsevier.com/locate/jeurceramsoc

T–T–T behaviour of bioactive glasses 1–98 and 13–93

Susanne Fagerlund, Jonathan Massera, Mikko Hupa, Leena Hupa *

Process Chemistry Centre, Åbo Akademi University, Turku, Finland

Available online 18 November 2011

Abstract

In this work crystallization kinetics of bioactive glasses 1–98 and 13–93 are discussed. Within a certain temperature–time window these glasses can be hot worked into various products without interfering with crystallization. The crystallization was studied isothermally by heating glass plates at different temperatures for different times. Phases in the samples were studied through XRD and SEM analyses. The nucleation-like curves and crystallization characteristics were measured with DTA. The temperature of maximum nucleation was measured for glass 1–98 at 725 °C and for 13–93 at 700 °C. The activation energy of crystallization of both glasses was 280 kJ/mol. The Johnson–Mehl–Avrami exponent and the SEM micrographs of the samples suggested surface crystallization. The primary crystalline phase was wollastonite. The growth rate of the crystallized surface layer was 1 order of magnitude higher in the plates of 1–98 than in 13–93. The results can be utilized to optimize the parameters in hot-working of the glasses.
© 2011 Elsevier Ltd. All rights reserved.

Keywords: Glass; Biomedical application; Thermal properties; Hot-working

1. Introduction

Bioactive glasses with their composition in the wollastonite primary field can be hot worked into various products without crystallization at carefully controlled time–temperature conditions.[1] These glass compositions can for example be sintered to porous implants or drawn into continuous fibres.[1–5] Further, tissue engineering scaffolds with strut structure sintered of powdered fractions of bioactive glasses have been reported.[6,7] The bioactive glass fibres have been tested as reinforcing components in different composite structures together with biodegradable polymers.[8]

Depending on the product, the glass forming operations take place within certain viscosity ranges. However, due to their low silica content and thus highly depolymerized structure compared to traditional glasses, bioactive glass melts crystallize easily at viscosity ranges typically applied in glass forming. For example, in the manufacture of porous bodies by viscous flow sintering of powdered glass above the glass transition temperature, too long residence times in the temperature range giving optimal viscosity might lead to extensive crystallization. The upper limit for the crystallization range is characterized by the liquidus temperature. In rotational viscometer the typical bioactive glasses crystallized at much lower viscosity values than utilized in drawing of continuous fibres from glass melts.[9,10] This implies that the viscosity at the liquidus temperature of bioactive glasses is much lower than the liquidus of conventional soda-lime glasses or fibreglasses. In practice, the crystal growth rate below the liquidus temperature is a limiting factor in glass forming. Thus, the strong tendency of bioactive glass melts to crystallize calls for a better understanding of their crystallization kinetics. For practical purposes the crystallization can be described with time–temperature–transformation (T–T–T) curves.

The aim of this work was to give detailed information on the T–T–T behaviour in heating of two bioactive glasses 1–98 and 13–93. The bioactivity of both glasses has been verified by in vivo studies. Amorphous porous implants sintered of the glasses have been shown to bond to rabbit femur.[11] Originally, their oxide compositions were developed in order to allow versatile hot working properties.[11,12] However, in the working range both glasses are close to or partly within the temperature region in which they show high tendency to crystallize. The information obtained can be employed to adjust hot working parameters so that crystallization is avoided.

2. Experimental

2.1. Sample preparation

Bioactive glasses 1–98 and 13–93 were prepared from analytical grade reagents of Na_2CO_3, K_2CO_3, MgO, $CaCO_3$, H_3BO_3,

* Corresponding author. Tel.: +358 2 215 4563; fax: +358 2 215 4952.
E-mail address: leena.hupa@abo.fi (L. Hupa).

0955-2219/$ – see front matter © 2011 Elsevier Ltd. All rights reserved.
doi:10.1016/j.jeurceramsoc.2011.10.040

Table 1
Nominal glass composition (wt%).

Glass	wt%						
	Na_2O	K_2O	MgO	CaO	B_2O_3	P_2O_5	SiO_2
1–98	6	11	5	22	1	2	53
13–93	6	12	5	20	–	4	53

$CaHPO_4{\cdot}2(H_2O)$ and Belgian quartz sand. The batches were melted in a platinum crucible for 3 h at 1360 °C, cast, annealed, crushed and remelted to ensure homogeneity. The nominal oxide compositions of the glasses are given in Table 1. The glasses were crushed and sieved to give the size range fraction 300–500 μm for the thermal analysis and cut to monolithic samples (20 mm × 10 mm × 5 mm) for the isothermal heat treatment.

2.2. Thermal analysis

The glass transition temperature T_g and the crystallization temperature T_p were determined by Differential Thermal Analysis (Mettler Toledo TGA/SDTA851^e) at various heating rates (10, 15, 20, and 30 °C/min). The measurements were performed on 50 mg samples with the particle size 300–500 μm in platinum pans in an N_2 atmosphere. T_g was taken at the inflection point of the endotherm, obtained by taking the first derivative of the DTA curve; T_p was taken at the maximum of the exothermic peak.

The activation energy E_c associated with the crystallization temperature was determined using the Kissinger equation (1) for T_p values measured at the different heating rates[13]:

$$\ln\left(\frac{q}{T_p^2}\right) = -\frac{E_c}{RT_p} + \text{constant}, \tag{1}$$

where q is the heating rate; T_p is the crystallization temperature measured at the different heating rates, and R is the gas constant.

The Johnson–Mehl–Avrami (JMA) exponent was determined using Eq. (2) proposed by Augis and Bennett[14]:

$$n = \frac{2.5}{\Delta T_{FWHM}} \frac{T_p^2}{E_c/R}, \tag{2}$$

where n is the JMA exponent and ΔT_{FWHM} is the full width at half maximum of the DTA peak. The JMA exponent gives information about the dimensionality of the crystal growth. The semi-quantitative, nucleation-like curve was determined using the method proposed by Marotta et al.[15] The curve is based on heating samples up to several potential nucleation temperatures. The maximum of the exothermic peak in DTA curve was measured with (T_p) and without (T_p^0) an isothermal hold for 30 min at T, the potential nucleation temperature. A 20 °C/min heating rate was chosen to suppress the formation of nuclei during the heating of the glass. The nucleation-like curve (I_0) is then obtained by plotting $((1/T_p) - (1/T_p^0))$ as a function of T, as shown by Eq. (3):

$$\text{Ln}(I_0) = \frac{E_c}{R}\left(\frac{1}{T_p} - \frac{1}{T_p^0}\right) + \text{constant} \tag{3}$$

where I_0 is the steady state nucleation rate and E_c is the activation energy for crystallization which represents the minimum amount of energy to initiate a reaction.

2.3. Isothermal heat treatment

Monolithic samples (20 mm × 10 mm × 5 mm) of the glasses were heat treated isothermally in the 600–1000 °C temperature range for 10 min to 8 h. The samples were inserted into an electric furnace on a graphite holder at a preset temperature. Experiments were conducted in N_2 atmosphere. The temperature in the furnace was controlled with a separate thermocouple within ±5 °C of the preset value. The heat treatment time was calculated from the moment the sample reached the preset temperature, i.e., roughly 15 min after inserting the sample into the furnace. After the treatment the samples were cooled in air. Two parallel samples were measured for each time point and for some selected points six parallel measurements were performed.

The cross-section of the plate was imaged with optical microscope (LEICA) equipped with a digital camera. Scanning electron microscope equipped with electron dispersive X-ray analyser (FEG-SEM, LEO 1530 Gemini from Leo/EDXA from Thermo Electron Corporation) was used to measure the average thickness of the crystallized layer and the composition of the phases in the samples. As the layers formed at the lower heat treatment temperatures and/or shorter times were not even, the thicknesses were measured in several locations for several plates. The values are given as arithmetical means with error bars indicating the minimum and maximum thicknesses.

Finally, the heat treated plates were ground to powder and the phase composition was analyzed using X-ray diffraction (X'pert by Philips, Cu α radiation, 40 kV, 30 mA, 5–60° 2θ, 0.8°/min). The diffractograms were analyzed using X'pert High Score, Powder Diffraction File database Data Sets 1–49 plus 70–86 (ICDD 1999). Powdered glasses of 1–98 and 13–93 prior to the heat treatment showed no signs of crystallization.

3. Results

3.1. The crystallization parameters with DTA

The DTA traces of 1–98 and 13–93 in Fig. 1, recorded at 20 °C/min heating rate, show an endothermic effect

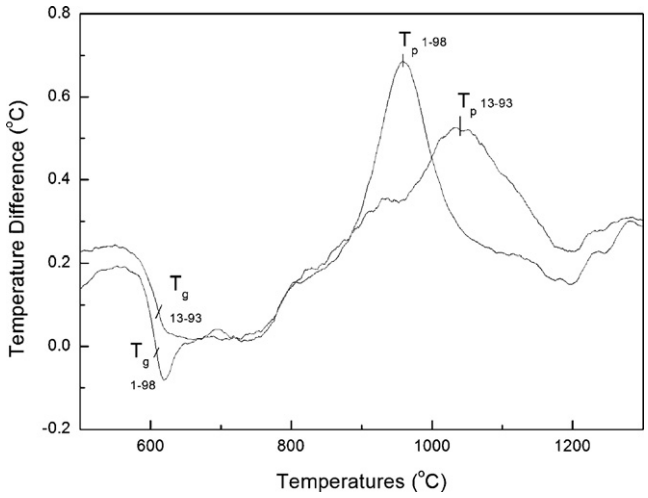

Fig. 1. DTA of 13–93 and 1–98 recorded at 20°/min.

corresponding to the glass transition temperature at 608 ± 5 °C (1–98) and 612 ± 5 °C (13–93), followed by an exothermic peak starting around 800 °C corresponding to the crystallization region. The maximum of the peak for 1–98 and 13–93 can be found at 958 ± 6 °C and 1038 ± 6 °C, respectively. The endothermic peaks within 1150–1250 °C give the melting of the crystals. Thus, these peaks can be used to estimate the liquidus temperature.

It is well known that T_p depends on the heating rate employed during the DTA measurement.[16] For samples of similar size, T_p shifts toward higher temperatures, when the heating rate is increased. Plotting $\ln(q/T_p^2))$ as a function of $1000/T$ gives a straight line which yields the slope $-E_c/R$ in Eq. (2).[13] For both glasses the activation energy for crystallization, E_c, was 280 ± 40 kJ/mol. The JMA parameter n, which is related with the growth dimensionality in crystallization, was close to 1 for both glasses.

The nucleation-like curves for the glasses are presented in Fig. 2. The nucleation domain for 1–98 was 700–760 °C and for 13–93, 680–730 °C. The error bars describe the accuracy of the DTA and the reproducibility of the measurements. Both

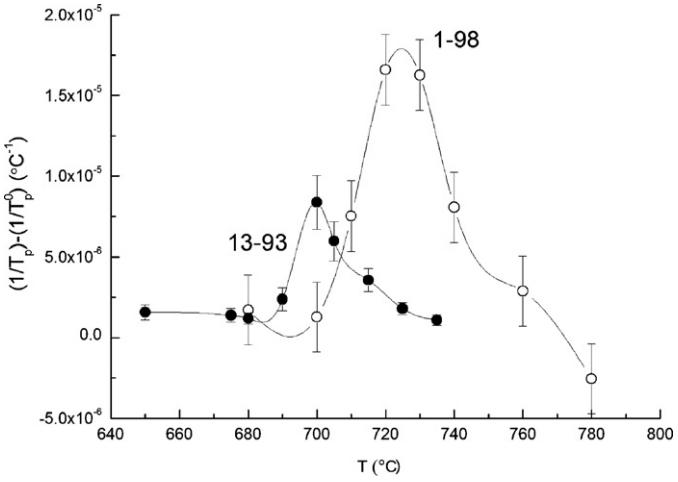

Fig. 2. Nucleation-like curves of 1–98 and 13–93.

curves exhibit a maximum, usually noted as the temperature of maximum nucleation ($T_{n\ max}$). The $T_{n\ max}$ for 1–98 and 13–93 was found at 725 °C and 700 °C, respectively. Even though the nucleation-like curves do not give the actual nucleation rates, these can be used as a good estimate of the actual ones. The differences in the $T_{n\ max}$ suggest that the nucleation rate for 1–98 is 10 times higher than for 13–93.

3.2. Crystallization characteristics for the monolithic samples

When heat treated at and above 800 °C all plates deformed to semi-spherical shape. The optical microscope images of the cross-sections of the samples show that the crystal growth started in the surfaces (Fig. 3). After longer heat treatments and higher temperatures, crystals were observed throughout the samples.

The first crystals in the surface of the glasses were detected after 1 h at 800 °C. Fig. 4 shows SEM micrographs of the surface of 1–98 and 13–93 after 1 h at 800, 900 and 1000 °C. The number of crystals in the surface of 1–98 at 800 and 900 °C is larger but their size is smaller than in 13–93. At 1000 °C only few and small crystals are seen in 1–98. In both glasses the crystals have a needle-like shape. The needles formed dendrites in both parent glasses.

The crystal composition of the needles was analyzed using XRD and SEM/EDX. Diffractograms of 1–98 and 13–93 heat treated at different conditions are given in Fig. 5. The peaks are typical for wollastonite ($CaSiO_3$). The two different polymeric sample holders used in the XRD experiment series caused relatively large variations in the amorphous region between 5 and 15 ° 2θ. Because the heat treated plates were pulverized prior the analysis no clear peaks were obtained with the samples having low fraction of crystalline phase. At 800 °C the crystal size was 20–40 μm in both glasses. The amount of crystals in 13–93 was still low at 900 °C, corresponding to a layer thickness around 400 μm. Clear wollastonite peaks recorded in the surface of 1–98 plates after heat-treatment at 800 °C have been reported earlier.[1] The insert in the figure shows a phase map (EDXA) of glass 1–98 heat treated at 920 °C for 1 h. The sample consists of glassy phase and crystals. According to the elemental chart calcium and silicon are the main elements in the crystalline phase.

The cross-sections of 1–98 and 13–93 after one hour at 900 and 1000 °C are shown in Fig. 6. The crystals showed branching texture in both glasses. The heat treatment temperature affected the branching; the lower the temperature the more the branching. Thus, the crystals formed at low temperatures assumed a sheaf-like shape. The crystal form did not change with prolonged heat treatment.

Fig. 7 shows the thickness of the crystallized layer in the glasses as a function of time at 900 °C. The layer thickness grew linearly with time in the glasses. Similar behaviour was observed at all temperatures. The R^2 for the measurements was between 85 and 99. The temperature dependency of the crystal layer growth was found to obey exponential behaviour in the studied temperature interval. The average crystal growth rate ($U_{average}$) as a function of temperature is shown in Fig. 8. The crystallization

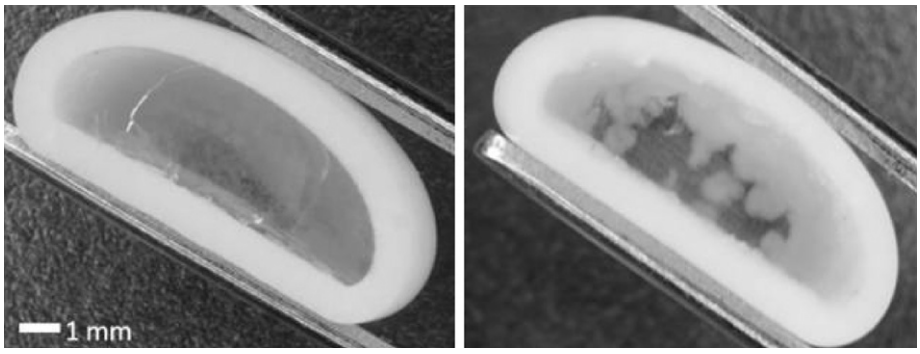

Fig. 3. Cross-sectional images of 1–98 (1 h, left) and 13–93 (4 h) after heat treatment at 900 °C.

rate of 13–93 was roughly 1 order of magnitude slower than that of 1–98 within the temperature range studied.

3.3. Empirical models for the crystal growth

Eq. (4) for glass 1–98 and Eq. (5) for the glass 13–93 were formulated based on the experimental results:

$$X(\mu m) = \left(\frac{t}{s}\right) \cdot (3 \times 10^{-11} \cdot e^{0.0257 \cdot T(^{\circ}C)}) \quad (4)$$

$$X(\mu m) = \left(\frac{t}{s}\right) \cdot (2 \times 10^{-11} \cdot e^{0.0241 \cdot T(^{\circ}C)}) \quad (5)$$

where X is the crystal layer thickness, t time, and T temperature. The equations can be used to estimate the crystal layer thickness as a function of the heat treatment time and temperature. It should be observed that they are valid only in the studied temperature interval; at higher temperatures a decrease in the crystal growth is expected.

4. Discussion

The crystallization of both glasses was found to commence around 800 °C. This was detected both with samples studied using DTA and samples heat treated in the electrical laboratory

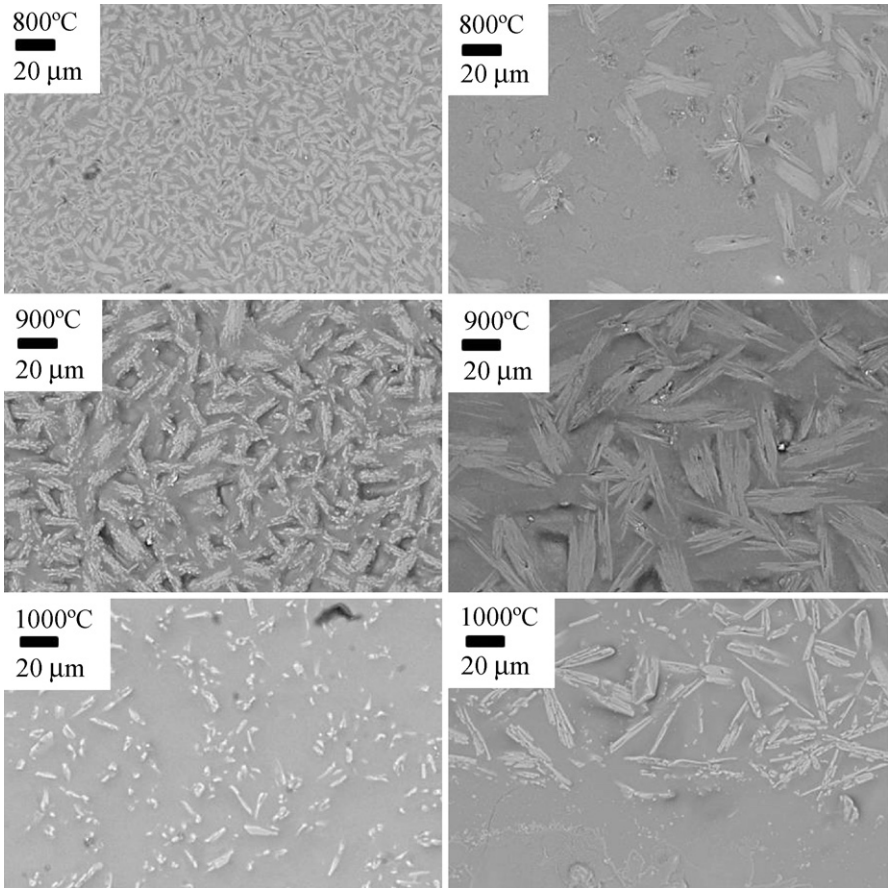

Fig. 4. SEM micrographs of surfaces of 1–98 (left) and 13–93 after 1 h at different temperatures.

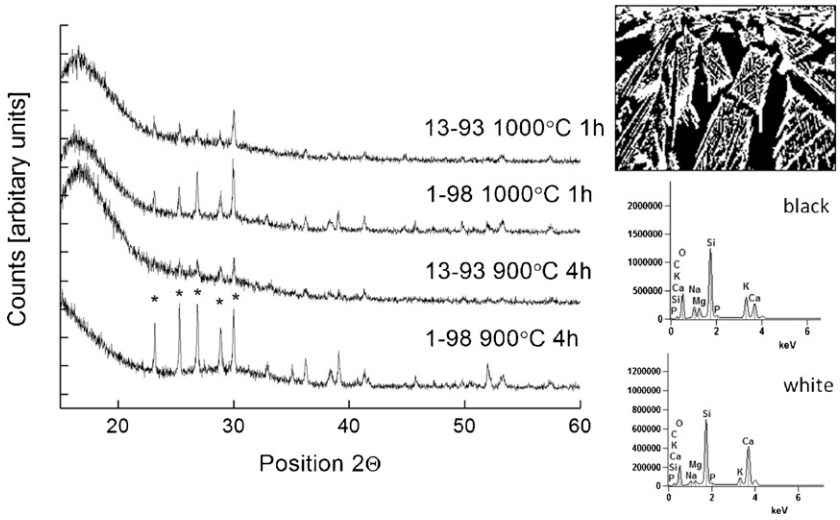

Fig. 5. Diffractograms of 1–98 and 13–93 heat treated at different conditions. The peaks are typical for wollastonite ($CaSiO_3$). The EDX phase map shows two phases in 1–98 after 1 h at 920 °C. The elemental analysis shows the composition of the phases (black = glass, white = crystal).

furnace. At this temperature the thermal properties clearly changed and the samples shape deformed. The deformation was likely due to minimization of the surface area of the bulk glass melt via viscous flow. Crystallization started from all surfaces, as confirmed by the optical microscope images. JMA value around 1 indicates a predominant surface crystallization.[17] Linear growth as a function of the heat treatment time indicates that the crystal tips grew toward fresh glass of constant composition. This implies interface controlled crystallization mechanism.[18] The activation energy for the crystallization was of the same order for the glasses. This suggests that the primary crystalline phase is identical for both compositions, as was also verified by the XRD and SEM analyses. The activation energy suggests further that as soon as the temperature reaches the onset for crystallization of the respective glasses, the initial crystal growth should occur at roughly same rate.

The similar JMA and activation energy values for crystallization suggest that same crystal type with the same dimensionality formed in both glasses. This result was also verified by the SEM and XRD analyses. Thus, the differences observed in the size and number of the crystals is assumed to depend on differences in the crystal nucleation and growth parameters in the two glasses. The number and size of the crystals in isothermal heat treatment depend on the degree of the overlapping of the nucleation and

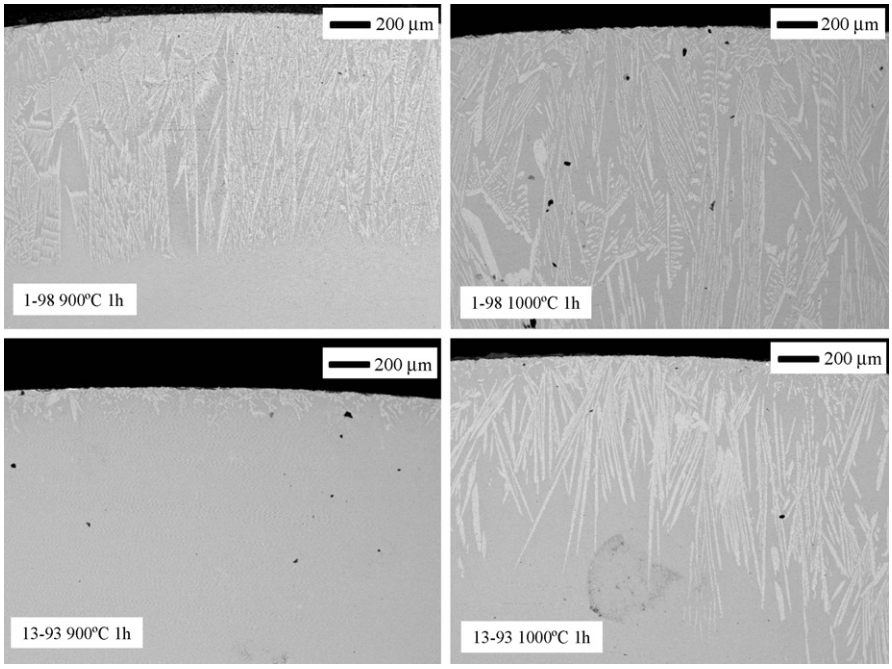

Fig. 6. SEM images of cross-sections of 1–98 and 13–93 after 1 h at 900 and 1000 °C (same magnification in all images).

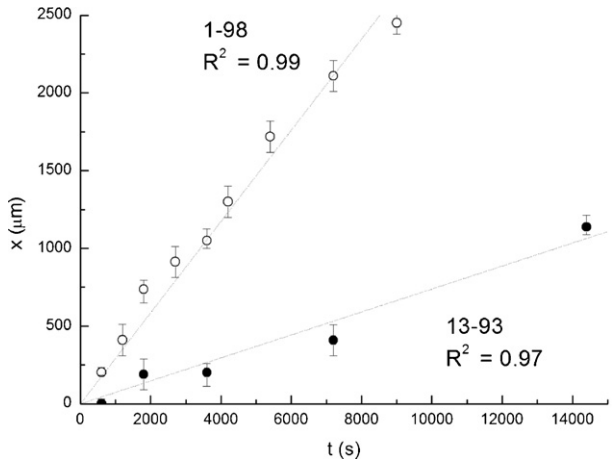

Fig. 7. Crystal layer thickness (x, μm) as a function of time at 900 °C for 1–98 and 13–93.

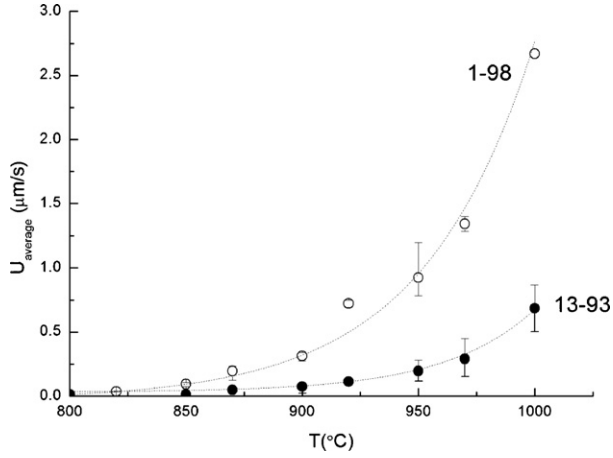

Fig. 8. Average crystal growth rate ($U_{average}$, μm/s) as a function of temperature for 1–98 and 13–93. The lines are drawn to guide the eye.

crystal growth domains but also on the number of quenched in nuclei. On another hand the size of the crystals depends mainly on the crystal growth rate.

In this study the nucleation-like curve was determined using the method proposed by Marotta et al.[15] Fig. 2 suggests that the temperature of maximum nucleation rate is at higher temperature for 1–98 than for 13–93. Further, the nucleation domain of 1–98 was broader and possessed higher amplitude than 13–93. Although Marotta's technique does not provide a real nucleation rate, the higher amplitude of the nucleation-like curve of 1–98 is often taken as an indication of a higher nucleation rate.

In this study no clear overlapping of nucleation and growth domains was observed for glass 13–93. However, in samples of 1–98 heat treated above 800 °C the density of crystals was lower than in samples heat treated at lower temperatures. This can be explained by a lower amount of nuclei available in samples rapidly heated to the higher temperatures. Thus, the relative number of crystals in the samples after the heat treatments can be used to estimate the overlap of the nucleation and crystal growth domains. The small degree of overlap at 800 °C for 1–98 is further confirmed by the pronounced decrease in the nucleation-like curve between 760 and 780 °C. Such decrease after the maximum domain in the nucleation-like curve is characteristic for a glass showing clearly separate domains for nucleation and crystal growth. The more rapid crystal growth rate in 1–98 than 13–93 explains partly the reported differences in the fibre drawing properties of the glasses.[19] When fibres were drawn below the liquidus, 1–98 crystallized faster than the 13–93. The slow growth rate in 13–93 allowed for the manufacture of continuous fibres, while crystallization faster prohibited the fibre drawing from glass melt 1–98.

The crystal layer thicknesses calculated with Eq. (4) and (5) are drawn as functions of both heat treatment time and temperature in a 3D plot in Fig. 9. The figure illustrates the large difference in the crystal growth rate for the two glasses. Eqs.

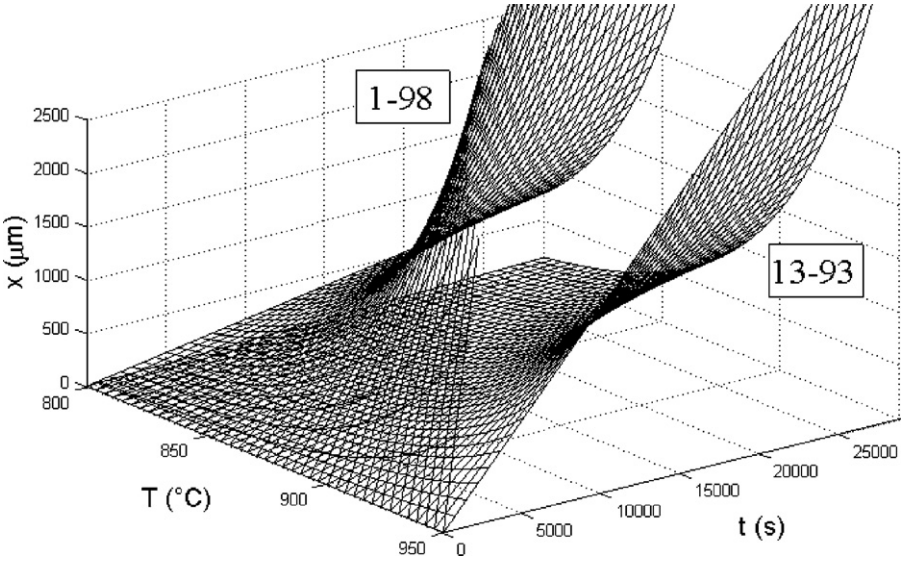

Fig. 9. Crystal growth as a function of time and temperature calculated with Eqs. (4) and (5).

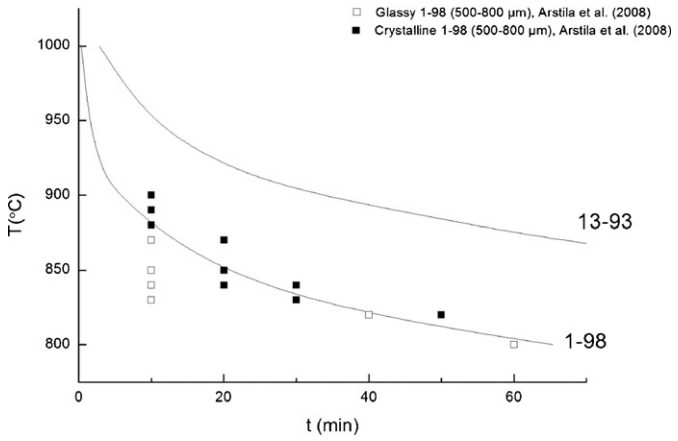

Fig. 10. T–T–T graph calculated using Eqs. (4) and (5). Threshold between glass and crystal layer assumed 100 μm.

(4) and (5) were utilized to draw T–T–T curves for the glasses. According to the SEM images it appears that the crystal layer should be around 100 μm to cover the entire sample surface. This value was used as a boundary between conditions for crystalline and amorphous phases when drawing the approximate T–T–T curves in Fig. 10. Thus, at the conditions below the lines the glasses do not crystallize, while at the conditions above the lines crystallization is expected to take place. In the same figure the experimental values from Arstila et al.[1] for the crystallization of particles (500–800 μm) of glass 1–98 are given. A good correlation can be found between the values reported for the crystallization of the particles and the obtained T–T–T curve for 1–98.[1] The T–T–T curve suggests that monolithic sampler of large particles of 1–98 can be heat treated below 800 °C for several hours and below 850 °C for at least 20 min before it starts to crystallize. Within 800–850 °C the viscosity of the melt is low enough to allow viscous flow sintering into porous bodies.[9] However, at the temperature range from 850 to 1000 °C the melt crystallizes easily. Glass 13–93 allows clearly longer hot-working times than 1–98 as suggested by Fig. 10. The T–T–T curves suggested can be used to estimate the parameters for glass processing within the temperature range from glass transition up to liquidus.

5. Conclusions

The crystallization characteristics essential for estimating the hot-working parameters of bioactive glasses 1–98 and 13–93 were studied. For both glasses the activation energy for crystallization was 280 kJ/mol. The temperature of maximum nucleation was measured at 725 °C for 1–98 and 700 °C for 13–93. The nucleation domain for 1–98 was found to be wider than 13–93 and the nucleation rate approximately 10 times higher. Thermal analysis suggested liquidus within 1150–1250 °C for both glasses. Johnson–Mehl–Avrami exponent SEM and XRD analyses of the isothermally treated samples suggested surface crystallization of wollastonite in both compositions. However, clear differences in their crystallization kinetics were observed. Although both glasses can be hot worked to amorphous products at carefully controlled conditions, 1–98 showed 1 magnitude greater crystal growth rate than 13–93. Thus, 13–93 is suited better than 1–98 for working processes which require long residence times at high temperatures. For instance, manufacturing of scaffolds by using organic sacrificial templates requires extended heat treatment to burn-out the organic matrix. The lower nucleation temperature and rate as well as lower crystal growth rate of glass 13–93 also suggest that this composition can be drawn into continuous fibres below liquidus.

Acknowledgements

The National Centre of Excellence Programme by the Academy of Finland, the Graduate School of Chemical Engineering, and Åbo Akademi Foundation are acknowledged for financial support.

References

1. Arstila H, Hupa L, Karlsson KH, Hupa M. Influence of heat treatment on crystallization of bioactive glasses. *J Non Cryst Solids* 2008;**354**(2-9):722–8.
2. Arstila H, Vedel E, Hupa L, Hupa M. Predicting physical and chemical properties of bioactive glasses from chemical composition. (II) Devitrification characteristics. *Glass Technol: Part A* 2008;**49**(6):260–5.
3. Arstila H, Tukiainen M, Hupa L, Ylänen H, Kellomäki M, Hupa M. In vitro reactivity of bioactive glass fibers. *Adv Sci Technol* 2006;**49**:246.
4. Laattala K, Huhtinen R, Puska M, Arstila H, Hupa L, Kellomäki M, et al. Bioactive composite for keratoprosthesis skirt. *J Mech Behav Biomed*, doi:10.1016/j.jmbbm.2011.05.025, in press, Corrected Proof.
5. Pirhonen E, Törmälä P. Coating of bioactive glass 13–93 fibres with biomedical polymers. *J Mater Sci* 2006;**41**(7):2031–6.
6. Chen QZ, Thompson ID, Boccaccini AR. 45S5 Bioglass®-derived glass–ceramic scaffolds for bone tissue engineering. *Biomaterials* 2006;**27**(11):2414–25.
7. Mantsos T, Chatzistavrou X, Roether JA, Hupa L, Arstila H, Boccaccini AR. Non-crystalline composite tissue engineering scaffolds using boron-containing bioactive glass and poly(D,L-lactic acid) coatings. *Biomed Mater* 2009;**4**(5):055002.
8. Alm JJ, Frantzén JPA, Moritz N, Lankinen P, Tukiainen M, Kellomäki M, et al. In vivo testing of a biodegradable woven fabric made of bioactive glass fibers and PLGA80—a pilot study in the rabbit. *J Biomed Mater Res B: Appl Mater* 2010;**93B**(2):573–80.
9. Vedel E, Arstila H, Ylänen H, Hupa L, Hupa M. Predicting physical and chemical properties of bioactive glasses from chemical composition, Part I: Viscosity characteristics. *Glass Technol: Part A* 2008;**49**(6):251–9.
10. Wallenberger FT, Smrcek A. The liquidus temperature; its critical role in glass manufacturing. *Int J Appl Glass Sci* 2010;**1**(2):151–63.
11. Itälä A, Koort J, Ylänen H, Hupa M, Aro H. Biologic significance of surface microroughing in bone incorporation of porous bioactive glass implants. *J Biomed Mater Res* 2003;**67A**(2):496–503.
12. Brink M. The influence of alkali and alkaline earths on the working range for bioactive glasses. *J Biomed Mater Res* 1997;**36**:109–17.
13. Kissinger HE. Reaction kinetics in differential thermal analysis. *Anal Chem* 1957;**29**(11):1702–6.
14. Augis JA, Bennett JE. Calculation of the Avrami parameters for heterogeneous solid state reactions using a modification of the Kissinger method. *J Therm Anal Calorim* 1978;**13**(2):283–92.
15. Marotta A, Buri A, Branda F. Nucleation in glass and differential thermal analysis. *J Mater Sci* 1981;**16**(2):341–4.

16. Moynihan CT. Correlation between the width of the glass transition region and the temperature dependence of the viscosity of high-T_g glasses. *J Am Ceram Soc* 1993;**76**(5):1081–7.
17. Christian JW. *The theory of metals and alloys*. Oxford: Pergamon Press; 1965.
18. Dillon SJ, Harmer MP. Diffusion controlled abnormal grain growth in ceramics. *Mater Sci Forum* 2007;**558 & 559**:1227–36.
19. Arstila H, Tukiainen M, Taipale S, Kellomäki M, Hupa L. Liquidus temperatures of bioactive glasses. *Adv Mater Res* 2008;**39–40**: 287–92.